



**HAL**  
open science

# Energy calibration of ion-beam accelerators with neutron and gamma nuclear reactions between 2 MeV and 4 MeV

Stéphanie Sorieul, Vincent Gressier

► **To cite this version:**

Stéphanie Sorieul, Vincent Gressier. Energy calibration of ion-beam accelerators with neutron and gamma nuclear reactions between 2 MeV and 4 MeV. Nuclear Instruments and Methods in Physics Research Section A: Accelerators, Spectrometers, Detectors and Associated Equipment, 2021, 489, pp.50-57. 10.1016/j.nimb.2020.12.007 . hal-03110857

**HAL Id: hal-03110857**

**<https://hal.science/hal-03110857>**

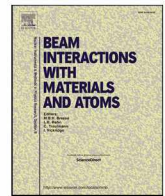
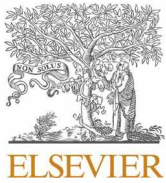
Submitted on 14 Jan 2021

**HAL** is a multi-disciplinary open access archive for the deposit and dissemination of scientific research documents, whether they are published or not. The documents may come from teaching and research institutions in France or abroad, or from public or private research centers.

L'archive ouverte pluridisciplinaire **HAL**, est destinée au dépôt et à la diffusion de documents scientifiques de niveau recherche, publiés ou non, émanant des établissements d'enseignement et de recherche français ou étrangers, des laboratoires publics ou privés.



Distributed under a Creative Commons Attribution - NonCommercial - NoDerivatives 4.0 International License



# Energy calibration of ion-beam accelerators with neutron and gamma nuclear reactions between 2 MeV and 4 MeV

St. Sorieul<sup>a,\*</sup>, V. Gressier<sup>b</sup>

<sup>a</sup> Université Bordeaux, CNRS-IN2P3, CENBG, Gradignan, France

<sup>b</sup> IRSN, BP3, Saint Paul lez Durance, France

## ARTICLE INFO

### Keywords:

Ion beam energy calibration  
Electrostatic accelerator  
<sup>27</sup>Al(p,γ)<sup>28</sup>Si resonances  
<sup>45</sup>Sc(p,n)<sup>45</sup>Ti resonance

## ABSTRACT

The accurate knowledge of the beam energy is of first importance in most applications using ion beams delivered by electrostatic accelerators. Regular beam energy calibration is thus required. The standard procedure is to use neutron thresholds and well known gamma-ray resonances. However, only a few calibration points are available between 2 MeV and 4 MeV despite the need of such beam energies, for instance, for nuclear reaction analyses.

In this work, the suitability of <sup>27</sup>Al(p,γ)<sup>28</sup>Si and <sup>45</sup>Sc(p,n)<sup>45</sup>Ti resonances has been studied in this specific energy range by comparison with well-established calibration energies. The methodology used for the experiments and data treatment is fully detailed.

The usefulness of these resonances is shown through several calibration campaigns that led to a complete energy calibration of two accelerator based facilities from 500 keV up to 4 MeV.

## 1. Introduction

Nowadays electrostatic accelerators are used for a large range of applications such as material analysis [1,2], cross-section measurements [3], neutron production or test of detection setup [4]. It is of first importance to know the energy of the incoming particles for all these applications. The energy of the accelerated ion ensures, for instance, a good control of the penetration depth of the ion to properly analyze the samples during resonant analysis. Furthermore, the knowledge of the energy beam is mandatory when accelerators are used for the test or the calibration of particle detectors as well as for nuclear reaction cross section measurements [5]. Finally, in ion beam analysis, the uncertainty on energy is a non-negligible part of the total uncertainty budget that has to be reduced as most as possible for quantifying the elements in analyzed samples.

Relying only on the terminal high voltage is generally not sufficient for electrostatic accelerators. In modern facility, a magnetic spectrometer (i.e. analyzing or analysis magnet) is often used with or without a NMR probe to assess the ion beam energy [6]. Sometimes the accelerator high voltage is determined by the use of Generating Voltmeter Motor (GVM) for an efficient stabilization. Therefore, the ion beam energy

calibration corresponds to the calibration of the analyzing magnet or/and of the GVM, as in [7], in a first place.

The calibration is most of the time performed using well-known neutron thresholds and gamma-ray resonances. Extensive efforts were done to provide accurate data during the 60's & 70's. Most of articles refer to neutron thresholds and gamma-ray resonances induced by protons beams at low energy up to 6 MeV, and by deuterium and alpha particles for higher energies up to 60 MeV [8–12]. The progressive improvement of the technology used for energy stabilization, beam transport, and detection allowed establishing a list of recommended reactions given with an excellent accuracy as shown in Table 1. The energy of some γ-ray resonances was measured accurately and neutron threshold energies depend mainly on the atomic mass. The broad selection of reactions make possible to precisely define the energy behavior of the analyzing magnet in a reproducible way. However, only a few reactions<sup>1</sup> are recommended for calibration between 2 MeV and 4 MeV. That lack of usable reactions is a drawback as a large number of resonant or scattering reactions used in ion beam analysis occurs in this energy range.

In the past twenty years, accelerator calibration was mainly performed between 1 MeV and 2 MeV [26–28] on the basis of the pioneer

\* Corresponding author.

E-mail address: [sorieul@cenbg.in2p3.fr](mailto:sorieul@cenbg.in2p3.fr) (St. Sorieul).

<sup>1</sup> The neutron threshold energies at 2168 keV and 2908 keV, respectively for <sup>65</sup>Cu(p,n) and <sup>45</sup>Sc(p,n) reactions, are not considered in this work due to the very low neutron production just above the threshold value.

**Table 1**

Summary of the recommended reactions below 4 MeV. In case of  $\gamma$ -ray resonances, the natural width is also given. Neutron threshold values are those obtained with Qcalc calculator [Qcalc] based on the latest atomic masses evaluation [13].

| Reaction                               | Ion energy (keV)       | Resonance natural width (keV) | Reference |
|--|------------------------|-------------------------------|-----------|
| $^{11}\text{B}(p,\gamma)^{12}\text{C}$ | $163.1 \pm 0.4$        | $5.3 \pm 1.0$                 | [14,15]   |
| $^{19}\text{F}$                        | $340.46 \pm 0.04$      | $2.34 \pm 0.04$               | [8,16]    |
| $(p,\alpha\gamma)^{16}\text{O}$        |                        |                               |           |
| $^{27}\text{Al}$                       | $632.23 \pm 0.04$      | $0.0048 \pm 0.0004$           | [17,18]   |
| $(p,\gamma)^{28}\text{Si}$             |                        |                               |           |
| $^{27}\text{Al}$                       | $991.756 \pm 0.017$    | $0.100 \pm 0.015$             | [12,18]   |
| $(p,\gamma)^{28}\text{Si}$             |                        |                               |           |
| $^3\text{H}(p,n)^3\text{He}$           | $1018.8751 \pm 0.0015$ | –                             | [13]      |
| $^{27}\text{Al}$                       | $1316.87 \pm 0.03$     | $0.070 \pm 0.035$             | [12,18]   |
| $(p,\gamma)^{28}\text{Si}$             |                        |                               |           |
| $^{27}\text{Al}$                       | $1587.49 \pm 0.08$     | $< 0.200$                     | [17]      |
| $(p,\gamma)^{28}\text{Si}$             |                        |                               |           |
| $^{13}\text{C}(p,\gamma)^{14}\text{N}$ | $1746.618 \pm 0.017$   | $0.135 \pm 0.008$             | [20,21]   |
| $^{27}\text{Al}$                       | $1799.75 \pm 0.09$     | $< 0.200$                     | [17]      |
| $(p,\gamma)^{28}\text{Si}$             |                        |                               |           |
| $^7\text{Li}(p,n)^7\text{Be}$          | $1880.36 \pm 0.08$     | –                             | [13]      |
| $^{11}\text{B}(p,n)^{11}\text{C}$      | $3016.99 \pm 0.07$     | –                             | [13]      |
| $^{13}\text{C}(p,n)^{13}\text{N}$      | $3235.48 \pm 0.29$     | –                             | [13]      |
| $^{15}\text{N}(p,n)^{15}\text{O}$      | $3774.05 \pm 0.52$     | –                             | [13]      |

works of Marion [8] and Bondelid & Dowling-Whiting [19]. Scarce publications mentioned less conventional methodologies such as the use of resonant or non-resonant scattering reactions to reach higher energies [29–32]. Those reactions are an interesting alternative but can have larger uncertainties mainly because of the imperfect knowledge of the target composition. Recently, Panetta et al. [33] investigated the usefulness of the  $^{32}\text{S}(p,\gamma)^{32}\text{S}$  reaction for energy around 3.4 MeV. Csedreki et al. [34] extended the use of  $(p,p'\gamma)$  reaction on  $^{28}\text{Si}$  and  $^{14}\text{N}$  to propose new calibration points at  $3100.6 \pm 0.9$  keV,  $3338.1 \pm 1.0$  keV,  $3903.1 \pm 1.7$  keV, and  $3991.6 \pm 1.1$  keV.

We propose to study additional accurate and reliable reactions in the 2 – 4 MeV range. The suitable reaction selection has to be based on several criteria such as their strength, their natural width, the good separation (at least a few keV) from other resonances, and an energy range where large structures due to photons or neutrons production by other reaction does not affect the measurements. As shown in this work, several  $^{27}\text{Al}(p,\gamma)$  resonances [35] satisfy the previously enumerated criteria. One of the challenge is that, above 2.3 MeV, the gamma emission from the  $^{27}\text{Al}(p,\gamma)^{28}\text{Si}$  resonances are mixed with those of the  $^{27}\text{Al}(p,p'\gamma)^{27}\text{Al}$  and  $^{27}\text{Al}(p,\alpha\gamma)^{24}\text{Mg}$  reactions [37,38]. The  $^{45}\text{Sc}(p,n)^{45}\text{Ti}$  first resonance [36] was also considered as it provides an additional calibration point at 2.9 MeV.

Ion beam energy calibrations were done at two separate facilities; one facility (AMANDE) is adequately equipped for neutron metrology with a strict control of the beam energy, the second one (AIFIRA) is equipped for analysis and irradiations with microbeams. The purpose of calibrating different facilities is to demonstrate the feasibility of our methodology for any accelerator of the community.

## 2. Experimental details

### 2.1. Description of the facilities

#### 2.1.1. AIFIRA

AIFIRA is an ion beam facility located at CENBG (Gradignan, France). The 3.5 MV Singletron™ (HVEE) accelerator that produces proton, deuteron and alpha beams with energy between 500 keV and 3.5 MeV is particularly well-adapted for focused microbeams. Its main activities are centered on ion beam analysis from microscopic to millimetric scale, targeted micro-irradiation with charged-particles at

cellular scale and the production of well-characterized monoenergetic neutron- and  $\gamma$ -fields.

The beam is transported from the accelerator to the analysis chamber or end-station via a  $90^\circ$  analyzing magnet, a switching magnet and one of the five beam lines [39]. The trajectory is defined thanks to two systems of slits (respectively called defining and stabilizing slits) and an aperture. The defining slits are situated before the magnet and help to set a preliminary beam position. Then, the passage through the aperture guarantees a good position of the beam in the x-direction into the  $90^\circ$  magnet. The stabilizing slits are implemented after the  $90^\circ$  magnet and connected to the Generating Voltmeter Motor (GVM). Energy stabilization and regulation are possible through the combined feedback of the GVM and stabilizing slits. The theoretical relative energy resolution of the accelerator is of  $2.5 \times 10^{-5}$ .

#### 2.1.2. AMANDE

The AMANDE facility, owned by IRSN and located at Cadarache (France), is based on a HVEE 2 MV Tandetron accelerator. Reference monoenergetic neutron fields are produced between 2 keV and 20 MeV energy using protons or deuterons beams sent on thin targets made of or containing scandium, lithium, deuterium or tritium [40]. These fields are mainly used for neutron metrology (French national standards) and calibration of neutron sensitive instruments. Ion beam energy is defined using a  $90^\circ$ -degree magnet. The magnetic field is precisely set by a computer controlled NMR teslameter; three Gauss gauges are placed at the centre of the magnet cavity which allows covering the required magnetic field range.

Beam position stabilizing slits in the x-plane are incorporated respectively at the object and image position that are located before and behind the  $90^\circ$  degree magnet. These slits, closed from 0.6 mm to a few mm depending on the settings, maintain the beam position control loops on respectively a X-steerer and the high voltage applied to the accelerator terminal measured with a GVM. The relative ion beam energy accuracy is of  $5 \times 10^{-4}$  as experimentally determined from reproducibility studies during several ion beam calibration campaigns performed over years [45].

### 2.2. Beam adjustment & End-station set-up

The beam energy  $E_p$  is tuned, for a given magnetic field  $B$  in the  $90^\circ$  magnet, a few keV above the energy  $E_0$  of the chosen neutron threshold or  $\gamma$ -ray resonance. Measurements at energies at least 2 keV above  $E_0$  have to be performed in order to have a sufficient energy range to fit the experimental data. The same beam adjustment procedure was performed for each calibration point:

- the desired field strength of the  $90^\circ$  magnet has always been approached from below,
- the stabilizing slits opening were sufficiently reduced to guarantee an excellent energy stabilization during the measurements.

The decrease of the beam energy is performed by applying a variable positive voltage  $V_T$  to a target electrically isolated from the rest of the beamline.

At AIFIRA, this voltage is supplied by a 0–20 kV high voltage power supply (Sefelec GKHT920P700) connected directly to the insulated target tube. This high voltage is remotely controlled by a source-meter. It is measured on the return signal by a calibrated voltmeter to take into account the voltage generated by the beam current on the target.

At AMANDE, a computer controlled 0–10 kV power supply (TREK 609B) is used with an isolated current converter that converts the intensity to a 0–10 V voltage. It is thus possible to apply a high voltage on the target (auto-compensated from the voltage generated by the ion beam on target) and to monitor the ion beam current value. The ion beam current, and the high voltage delivered by the TREK power supply are regularly calibrated on all the used range (from 1 nA to 100  $\mu\text{A}$ )

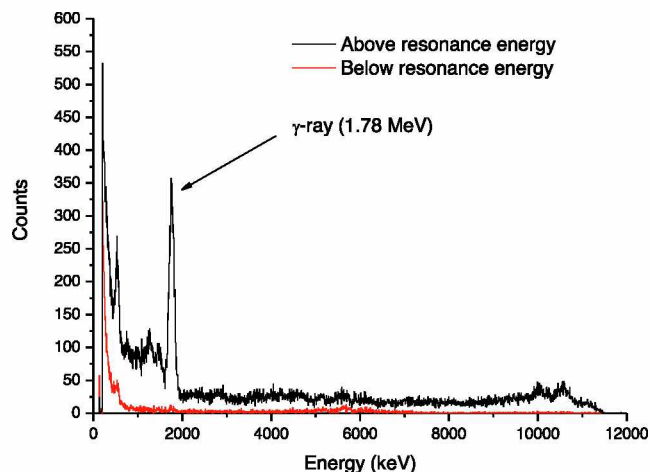


Fig. 1. Photon energy distribution determined by the BGO above and below the  $^{27}\text{Al}(p,\gamma)^{28}\text{Si}$  resonance at 992 keV with the clearly visible 1779 keV gamma line.

respectively with a standard current source and a multi-meter coupled to a HV probe (both of them being previously calibrated at a reference HV source). The uncertainties on beam current and high voltage are lower than respectively 0.5% (above 20 nA) and 0.2%.

The targets are mounted on the beam line devoted to neutron production at both facilities. They are cooled with a flux of compressed air and the beam current is kept below a few  $\mu\text{A}$ . During the calibration experiment, the slits systems are closed to 1 mm or lower in order to constraint the beam trajectory.

## 2.3. Detectors

### 2.3.1. Photons

The photon detector used to measure the  $\gamma$ -ray resonances has to cover an energy range between 1 MeV and at least 10 MeV. For this study, a commercial HARSHAW BGO spectrometer (type NR: 4S4/1.5 A – BX) with both a height and a diameter of 2.54 cm (1") is used. The photon energy range of this detector goes from 100 keV to 12 MeV. Given the high Z value of the material, the photo fraction for gamma ray absorption is high and, even for such a small size of scintillator, the peak-to-total ratio is good enough (0.55, 0.35 and 0.2 at respectively 1 MeV, 2 MeV and 4 MeV) for this study. Due to its relatively low efficiency, the BGO is placed at a few cm from the target and at  $0^\circ$  taking care to maintain dead time lower than 1% (determined from the ratio Live time/Real Time on the acquisition system). This detector is generally useful when the experimenters want to focus only on the reaction of interest by just selecting the energy range of the awaited photo-peaks in the pulse height spectra as shown in the Fig. 1. In this study, we used this detector as a simple counter by just setting a low discrimination level around 1 MeV to avoid the contribution of low energy photons. Indeed, following the variation of the counts on a fixed time interval as a function of the proton energy is enough to determine the resonance energies. However, the chosen threshold is not high enough to avoid all the contribution of the competing  $^{27}\text{Al}(p,p'\gamma)^{27}\text{Al}$  and  $^{27}\text{Al}(p,\alpha\gamma)^{24}\text{Mg}$  reactions that polluted the measurements.

### 2.3.2. Neutrons

At AMANDE, a long counter detector (PLC) based on a  $^3\text{He}$  tube was used for neutron detection [41]. This detector has a very flat response function [42] that does not vary by more than  $\pm 2.5\%$  around its mean value of  $9.5\text{ cm}^2$  on the energy range of the neutrons produced around the thresholds (6–90 keV). The front face of the PLC is placed at 30 cm from the target subtending a solid angle with a half angle of about  $34^\circ$ . However the angular response is not as flat as the energy one with more

Table 2

List of the used targets with indicative thicknesses as reported by manufacturers, and energy loss by protons.

| Target           | Thickness ( $\mu\text{g}/\text{cm}^2$ ) | Energy loss (keV) |
|------------------|---|-------------------|
| Ti               | 215                                     | 35                |
| $^7\text{LiF}$   | 45                                      | 6                 |
| $^{11}\text{B}$  | 40                                      | 4                 |
| $^{13}\text{C}$  | 95                                      | 10                |
| $^{15}\text{N}$  | 100                                     | 9                 |
| $^{27}\text{Al}$ | 115                                     | 8 to 13*          |
| $^{45}\text{Sc}$ | 1/27                                    | 0.075/2.0         |

\*in the 2–4 MeV proton energy range.

sensitivity in its axis (i.e. low angles) than at its borders (largest angles) reducing the usable half angle to about  $15^\circ$ .

For AIFIRA, the chosen detector was a 4.5' Bonner sphere, from IRSN HERMEIS system, with a  $^3\text{He}$  spherical proportional counter of 5.08 cm (2 in.) diameter filled with a pressure of 10 atm placed in the centre of the sphere. The neutron response of the 4.5' sphere (mean value of  $8.3\text{ cm}^2$ ) does not vary by more than  $\pm 7\%$  in the energy range of interest [43]. The detector was placed at 10 cm from the target leading to a subtended half angle of about  $30^\circ$ .

For both detectors, the events occurring in their sensitive volume are recorded via a Multi-Channel Analyser (MCA) after amplification. A threshold on the pulse height is applied to discriminate the electronics/gamma noise from the neutron events; the pulse height spectrum being mostly independent on the neutron energy distribution.

## 2.4. Targets

All the targets (except the  $^{15}\text{N}$  one) are made of a reactive thin layer deposited on a backing of tantalum (0.25 mm thick). The  $^{15}\text{N}$  target has been made by implantation with 10 keV  $^{15}\text{N}$  beam in the tantalum backing at SIDONIE facility [44]. The mean penetration depth is 14 nm but the range of implantation is up to 40 nm as  $^{15}\text{N}$  is in gaseous form. The used targets with their respective thickness are given in Table 2.

For the  $\gamma$ -ray resonances and the  $^{45}\text{Sc}(p,n)^{45}\text{Ti}$  first resonance, the thickness is chosen to ensure that the energy loss into the target is more than three time larger than the natural width of the resonance and the beam energy spread ( $\sim 0.5$  to 1 keV), i.e. at least 2 keV. Furthermore, and because it was available at AIFIRA facility, we also used a very thin scandium target of  $1\ \mu\text{g}/\text{cm}^2$  thickness providing the resonance energy directly from the peak obtained in the neutron yield. No real constraint exists on the thickness of target used for neutron threshold measurements. However the thickness should be sufficient so that the beam energy loss into the target is more than a few keV allowing a sufficient scan range to accurately determine the applied voltage at the threshold.

## 3. Calibration methodology

### 3.1. Energy correlation with the magnetic field

A charged particle path in a uniform and stationary magnetic field  $B$  is circular due to the Lorentz force. Taking into account relativist corrections, the relation between energy (in keV) and magnetic field generated by the  $90^\circ$  magnet (in mT) is:

$$E(E - mc^2) = (qcBR)^2 \quad (1)$$

The best method to define the beam energy is then to fix the trajectory of the beam (i.e. to fix  $R$ ). In such condition, there is a direct relation between energy of the particles and the magnetic field if  $B$  is measured in an absolute and precise way [11]:

$$E = k(E) \cdot B^2 \quad (2) \text{ with } k(E) \text{ called « magnet factor » and defined as:}$$

$$k(E) = \frac{10^3 q^2 R^2}{2m \left(1 + \frac{E}{2mc^2}\right)} = \frac{a}{\left(1 + \frac{E}{2mc^2}\right)} \quad \text{with } a = \frac{10^3 q^2 R^2}{2m} \quad (3)$$

For protons,  $q = 1$  (elementary charge =  $1.602 \times 10^{-19}\text{C}$ ) and  $m =$

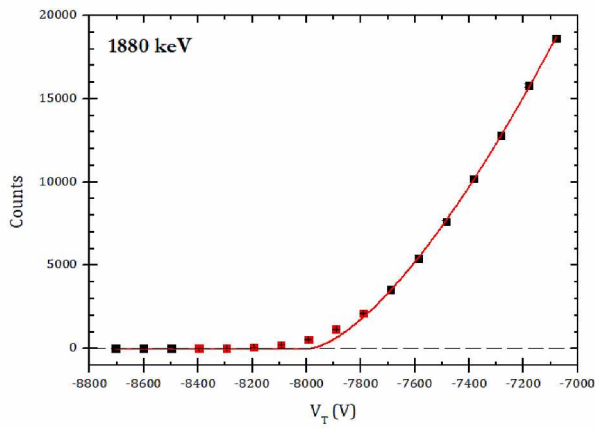


Fig. 2. Example of variation of the counts  $N$ , and  $N$  elevated to the power  $2/3$  just above the 1880 keV neutron threshold of the  ${}^7\text{Li}(p,n)$  reaction as a function of the voltage  $V_T$  applied to the target. Points in red are those rejected from the data fit. Fit curves are in red. (For interpretation of the references to colour in this figure legend, the reader is referred to the web version of this article.)

938272.013(23) keV/ $c^2$ . The previous equation becomes, with proton energy  $E_p$  in keV:

$$k(E_p) = \frac{a_p}{\left(1 + \frac{E_p}{1876544}\right)} \quad (4)$$

The proton beam energy  $E_p$  is determined by the direct relationship  $E_p = E_0 + V_0$ , with  $V_0$  being the voltage value to apply to reach the threshold or resonance energy. The magnet factor  $k(E_p)$  can then be deduced from equation (2) as :

$$k(E_p) = \frac{E_p}{B^2} = \frac{E_0 + V_0}{B^2} \quad (5)$$

The proton beam energy calibration aims therefore to determine the value of  $V_0$ .

To transfer the proton energy calibration to any type of ion beam, equation (3) is used with  $q_i$  and  $m_i$ , respectively the charge and mass of the accelerated ion of energy  $E_i$ :

$$k(E_i) = \frac{a_p q_i^2}{\left(\frac{m_i}{m_p} + \frac{E_i}{1876544}\right)} \quad (6)$$

### 3.2. Data analysis

The counts collected by the detector during a given time are recorded as a function of the high voltage  $V_T$  applied to the target. A fit is performed with OriginLabs software using different models adapted to the considered reaction and is weighted by the data statistical uncertainties.

#### 3.2.1. Neutron threshold

The energy dependence of the total cross-section, for neutron emission just above threshold, varies as  $(E-E_0)^{3/2}$  where  $E_0$  is the threshold energy. Experimental data are therefore fitted using a  $Y^{3/2}$  function as well as a linear fit of the counts elevated to the power  $2/3$  as shown in the Fig. 2.

Fits are performed by removing data just around the threshold due to the influence of the beam energy spread. This method is valid only if all the emitted neutrons reach the detector. Consequently, experimental data can be fitted only on a limited energy range depending on the reaction and on the covered solid angle. The voltage  $V_0$  extracted from the data analysis is the mean value of both fits. Its uncertainty takes into account the deviation between the two fitting methods.

#### 3.2.2. Resonances

Charged particles have a Gaussian-like energy distribution which can be defined by its mean energy and its width. The mean energy is considered as the energy of the beam whereas the width is its energy spread, mainly due to the fluctuation of the accelerator high voltage. For accelerators having a ‘‘tandem geometry’’ like AMANDE, it is correlated

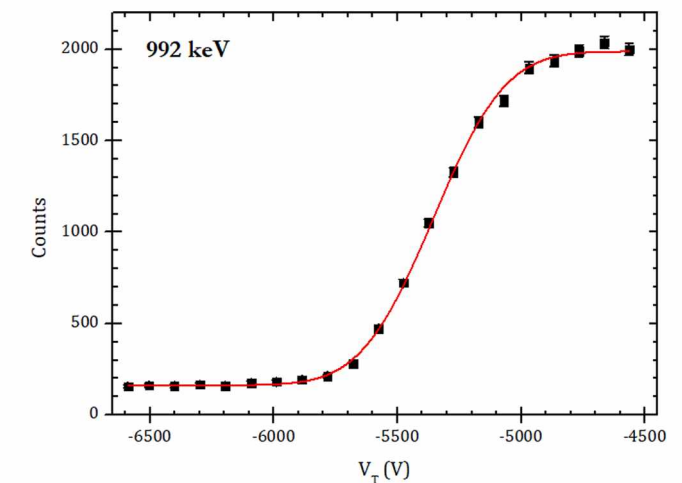
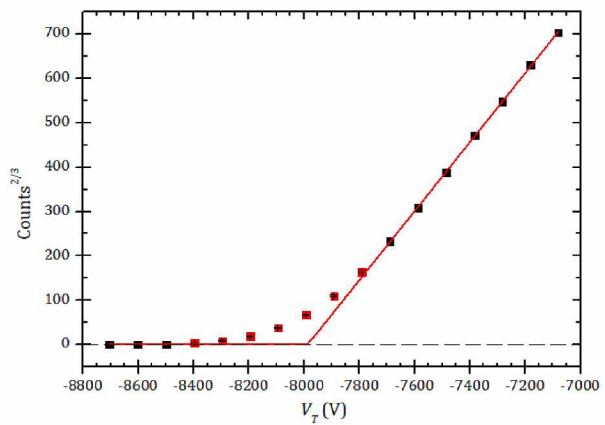


Fig. 3. Example of variation of the counts  $N$  around the 992 keV  ${}^{27}\text{Al}(p,\gamma)$  resonance as a function of the voltage  $V_T$  applied to the target. Fit curve is in red. (For interpretation of the references to colour in this figure legend, the reader is referred to the web version of this article.)

to the energy broadening effect induced by the ion beam interactions with the stripper canal leading to a beam energy width varying between 500 eV and 1 keV. The induced energy broadening does not allow to see the Lewis peak in the photon yield as a function of the proton energy. As a result and as  $\gamma$ -resonances have a Lorentz energy distribution, it is assumed that the experimental data are described by a cumulative Gaussian, as shown in Fig. 3, or Lorentz distribution if the resonance width is respectively smaller or larger by more than a factor 3 compare to the beam energy width.

## 4. New reactions in the 2–4 MeV range

### 4.1. ${}^{27}\text{Al}(p,\gamma)$ resonances

Above 2.3 MeV, large variations with energy of the photon production are observed in addition to the resonances. This is due to competing reactions in aluminum i.e.  ${}^{27}\text{Al}(p,p'\gamma)$  and  ${}^{27}\text{Al}(p,\alpha\gamma)$  [38] or in the target backing. Those variations could be reduced by selecting relevant photon energies in the recorded spectra. In the present measurements, only a low discrimination level has been applied to optimize count rates. Nevertheless, a confident fit by a cumulative Gaussian function can be obtained at 3960 keV, 3791 keV, 3338 keV, 3162 keV, 2675 keV, 2517

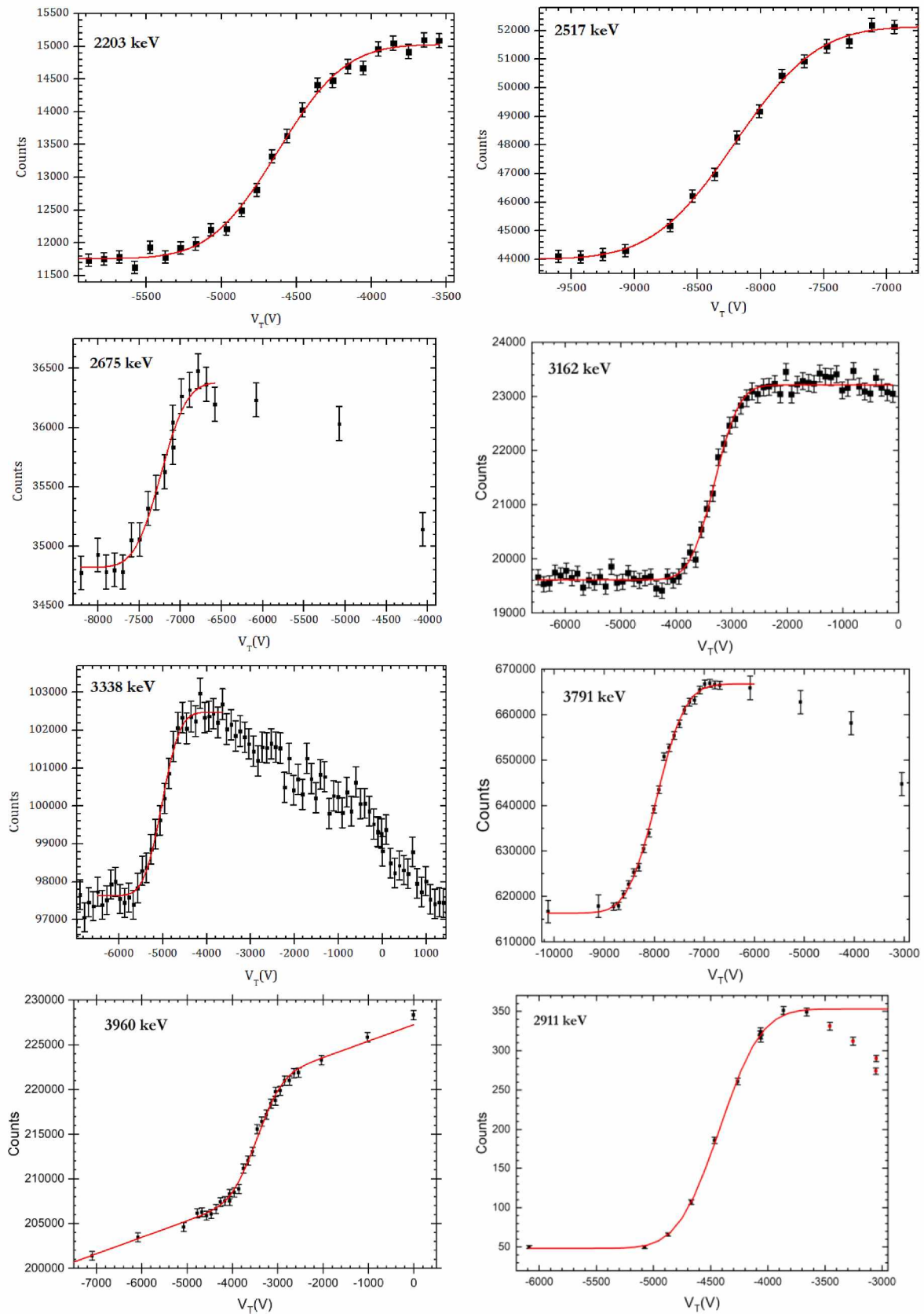
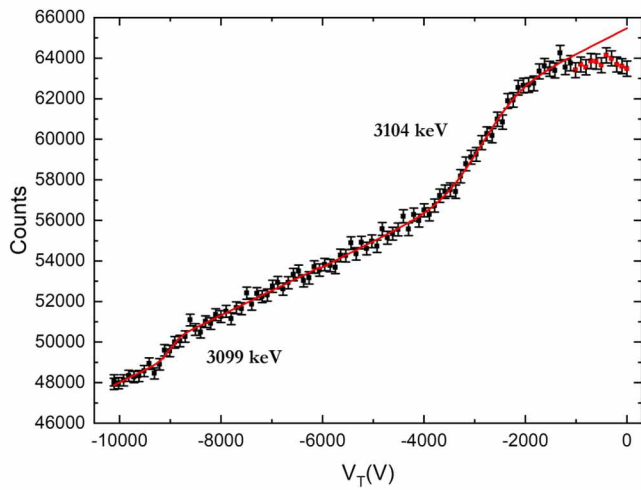
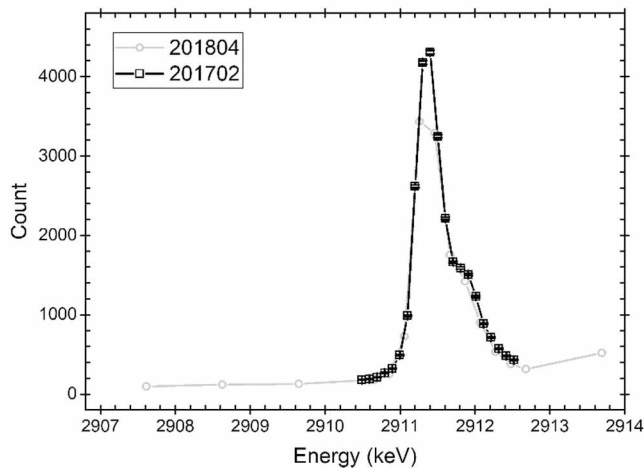


Fig. 4. Variations of the counts as a function of the applied voltage to the target for the  $^{27}\text{Al}(p,\gamma)$  and  $^{45}\text{Sc}(p,n)$  resonances as mentioned in the text. Measurements were performed at AMANDE facility. Fit curves are in red. (For interpretation of the references to colour in this figure legend, the reader is referred to the web version of this article.)



**Fig. 5.** Variations of the counts as a function of the applied voltage to the target for the  $^{27}\text{Al}(p,\gamma)$  3099 and 3104 keV resonances as mentioned in the text. Measurement performed at AMANDE facility. Fit curves are in red. (For interpretation of the references to colour in this figure legend, the reader is referred to the web version of this article.)



**Fig. 6.** Variation of the counts as a function of the ion beam energy for the first  $^{45}\text{Sc}(p,n)$  resonance. The energy was determined from AIFIRA accelerator Terminal voltage reduced by the applied voltage at the target.

keV and 2203 keV resonances [35]. Only the energies of the resonance are reported as their width are all negligible with respect to the proton beam energy width. The energy uncertainty on all these resonances is 1 keV as reported on the associated excitation energies in [35]. High statistics are required at 2675 keV and 3338 keV as the relative variation in the count rate before and after the resonance are respectively of only 4% and 5%. The latter resonance is very close to the 3338.1 keV  $^{28}\text{Si}(p,p'\gamma)$  one proposed by Csedreki et al. For the 3960 keV resonance, we improved the resonance fit by adding a linear correction defined just before and after the resonance. Fig. 4 shows the data fit of the considered  $^{27}\text{Al}(p,\gamma)$  resonances above 2 MeV as measured at AMANDE facility with the same target. The uncertainties on each point is calculated as the quadratic sum between the statistical uncertainty and the ion beam current uncertainty.

The 3099 keV, 3104 keV, and 3674 keV resonances have not been selected for energy calibration. Indeed the 3099 keV and 3104 keV resonances requires a linear correction that appears too important to get a reliable measurement, especially for the 3099 keV resonance as shown in the Fig. 5. More, the 3674 keV resonance was not observed using the present method. Further investigations are needed to understand this

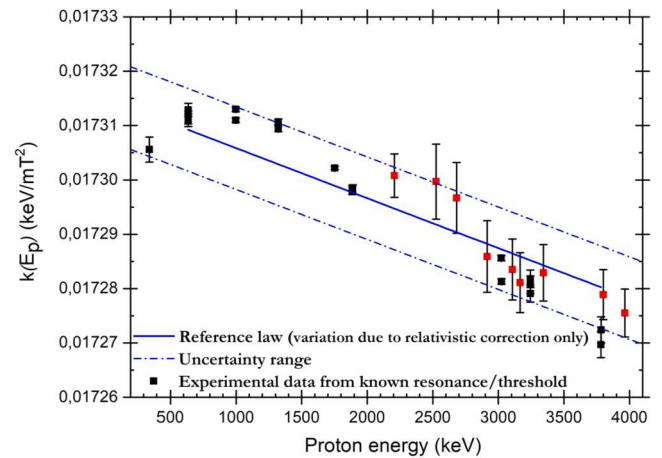


**Fig. 7.** Variation of AMANDE's magnet factor  $k(E_p)$  with the proton energy. In red the experimental values obtained with the new proposed  $^{27}\text{Al}(p,\gamma)$  resonances and the first  $^{45}\text{Sc}(p,n)$  resonance. (For interpretation of the references to colour in this figure legend, the reader is referred to the web version of this article.)

latter disagreement with literature.

#### 4.2. $^{45}\text{Sc}(p,n)$ resonance

First, the neutron threshold of the  $^{45}\text{Sc}(p,n)$  reaction is hardly usable because the neutron production is extremely low. However a suitable neutron emission can be obtained at the first  $(p,n)$  resonance. Indeed, the energy of the neutrons produced in the ion beam direction was accurately determined by time of flight as being  $8.12 \pm 0.01$  keV [46], close to the value in [47]. From kinematics, and using the uncertainty of the Q-value determined from Q-calc calculator, it corresponds to a proton energy of  $2911.1 \pm 1.1$  keV. The resonance energy can be used for calibration if the target is thick enough ( $20 \mu\text{g}/\text{cm}^2$  or more) or very thin.

At AMANDE facility, we used a scandium target of  $27 \mu\text{g}/\text{cm}^2$  thickness that is just enough to fit correctly the resonance with a cumulative Gaussian function: intensity decreases quickly 1 keV above the resonance as we can see in Fig. 4. At AIFIRA facility, very thin targets of about  $1 \mu\text{g}/\text{cm}^2$  were available. We deduced the resonance energy directly from the resonance peak summit applying a correction only for half of the mean proton energy loss in the scandium layer (i.e. 37 eV). Two measurements were performed (Fig. 6) respectively in February 2017 and April 2018. The resonance energy deduced from the accelerator voltage is similar for the two measurements. Nevertheless, the value is higher of about 0.3 keV compare to the reference energy.

#### 4.3. Validation of the new set of reactions

The energy calibration is performed every year at AMANDE facility using several energies given in Table 1. The linear variation with energy of the magnet factor  $k(E_p)$  is then fitted using equation (4). In order to validate the use of the new proposed energies, their corresponding  $k(E_p)$  values have been added to the Fig. 7.

In Fig. 7, the dotted lines delimit the relative maximum deviation of  $5 \times 10^{-4}$  considered on the magnet factor based on the reproducibility of several measurements performed over years [Cog10]. The reproducibility is possibly due to the magnetic field differential hysteresis into the  $90^\circ$  magnet, to deviations due to the energy regulation by the slits (due to its limited range), to the difference between the field at the NMR probe and the field really seen by the particles through their pathway into the magnet (any variation of beam focusing or alignment at the entrance of the magnet will modify the beam trajectory, i.e. its energy due to the control loop with the slits). It can also be observed that there

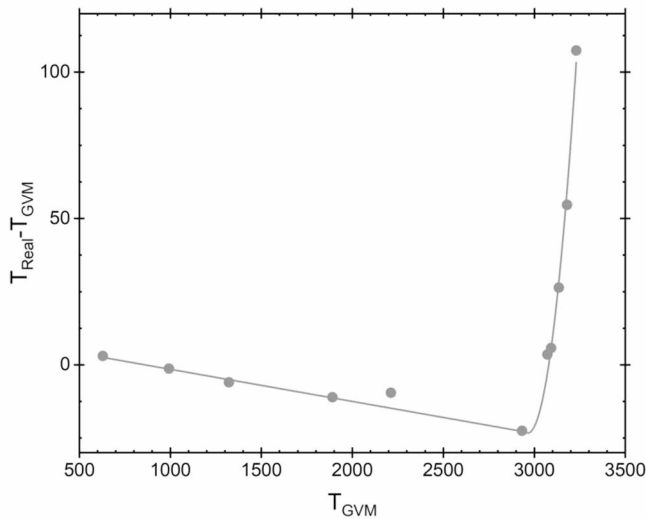


Fig. 8. Variation of  $TV_{\text{REAL}} - TV_{\text{GVM}}$  as a function of  $TV_{\text{GVM}}$  at AIFIRA facility.

may be a systematic deviation of  $k(E_p)$  from the linear variation indicating that the previously mentioned effects could depend on the beam energy. However, within the reproducibility uncertainty, the additional energy values show a good agreement with the reference linear law. The new proposed  $^{27}\text{Al}(p,\gamma)$  resonances and the first  $^{45}\text{Sc}(p,n)$  resonance seem therefore usable as reference energy points for proton beam energy calibration.

### 5. Example: calibration of AIFIRA accelerator

Several activities at AIFIRA facility require the accurate knowledge of the beam energy, for instance when a specific nuclear reaction has to be studied or for the depth profiling of a peculiar light element. Nevertheless, as for many other facilities, the accurate measurement of the magnetic field in the  $90^\circ$  magnet is not available. The main goal of the calibration is therefore to determine the relationship between the accelerator real terminal voltage ( $TV_{\text{Real}}$ ) and the voltage read by the GVM ( $TV_{\text{GVM}}$ ). Indeed, only this latter one is at the disposal of the operators during the beam tuning. Fig. 8 shows the variation of the difference between  $TV_{\text{Real}}$  and  $TV_{\text{GVM}}$  versus  $TV_{\text{GVM}}$ . Most of the threshold reactions and some resonance reactions were systematically performed at each run in order to assess the repeatability of the measurements.

As already observed at many others facilities [26–28], the correlation between  $TV_{\text{GVM}}$  and  $TV_{\text{Real}}$  is linear below  $\sim 3$  MeV. Above beam energy of around 2.9 MeV, the deviation between the two voltages seems to follow a second order polynomial law. This deviation of about 2.5% at 3.2 MeV was the primary reason why the authors were looking for alternative nuclear reactions useful for accelerator calibration. Indeed at the beginning of the AIFIRA calibration campaign, nearly four years ago, useful reactions around 3 MeV were scarce.

Such deviation was also observed by Wilkerson et al. [48] without explanation of its possible origins. On the basis of our exchanges with the accelerator manufacturer HVEE, two phenomena may occur for AIFIRA. The first possibility is the increase of the electrostatic forces in the terminal voltage that may decrease the distance between the GVM and the terminal. The result will be a lower tension voltage while the electrostatic field strength remains the same, i.e.  $TV_{\text{GVM}}$  will be lower than the real value delivered by the accelerator as observed in our measurements. The second phenomenon is that the GVM linearity is no more valid at high voltage combined with the fact that the  $TV_{\text{GVM}}$  readout on the CPU is less reliable than the value directly measured on the GVM. This linearity will be checked in a further study.

Table 3

Proposed new resonances for ion beam energy calibration between 2 MeV and 4 MeV.

| Reaction                                 | Ion energy (keV)   |                  |                      |
|--|--------------------|------------------|----------------------|
|  | Neutron threshold  | This work        | Csedreki et al. [34] |
| $^{27}\text{Al}(p,\gamma)^{28}\text{Si}$ |                    | $2202.5 \pm 1.0$ |                      |
| $^{27}\text{Al}(p,\gamma)^{28}\text{Si}$ |                    | $2517.3 \pm 1.0$ |                      |
| $^{27}\text{Al}(p,\gamma)^{28}\text{Si}$ |                    | $2675.1 \pm 1.0$ |                      |
| $^{45}\text{Sc}(p,n)^{45}\text{Ti}$      |                    | $2911.1 \pm 1.1$ |                      |
| $^{11}\text{B}(p,n)^{11}\text{C}$        | $3016.99 \pm 0.07$ |                  |                      |
| $^{28}\text{Si}(p,p')^{28}\text{Si}$     |                    |                  | $3100.6 \pm 0.9$     |
| $^{27}\text{Al}(p,\gamma)^{28}\text{Si}$ |                    | $3162.3 \pm 1.0$ |                      |
| $^{13}\text{C}(p,n)^{13}\text{N}$        | $3235.48 \pm 0.29$ |                  |                      |
| $^{27}\text{Al}(p,\gamma)^{28}\text{Si}$ |                    | $3337.9 \pm 1.0$ |                      |
| $^{28}\text{Si}(p,p')^{28}\text{Si}$     |                    |                  | $3338.1 \pm 1.0$     |
| $^{15}\text{N}(p,n)^{15}\text{O}$        | $3774.05 \pm 0.52$ |                  |                      |
| $^{27}\text{Al}(p,\gamma)^{28}\text{Si}$ |                    | $3791.1 \pm 1.0$ |                      |
| $^{14}\text{N}(p,p')^{14}\text{N}$       |                    |                  | $3903.1 \pm 1.7$     |
| $^{27}\text{Al}(p,\gamma)^{28}\text{Si}$ |                    | $3960.2 \pm 1.0$ |                      |
| $^{14}\text{N}(p,p')^{14}\text{N}$       |                    |                  | $3991.6 \pm 1.1$     |

### 6. Conclusion

The accurate knowledge of the beam energy is of first importance in most applications using electrostatic accelerators. Regular beam energy calibration is thus required. The standard procedure is to use neutron thresholds and well known gamma-ray resonances. However, only a few calibration points are available between 2 MeV and 4 MeV despite the need of such beam energies, for instance, for nuclear reaction analyses.

We have performed energy calibrations at two separate facilities with new energy points. The purpose of using two different facilities was to demonstrate that our methodology and the proposed reactions can be useful for any facility of the accelerator community.

Based on the calibration curves we obtained, a new set of energies for proton beam energy calibration in the 2 MeV – 4 MeV range is proposed. These additional energies have been successfully compared to the well-established calibration reference energies at AMANDE facility, proving the suitability of their use. Furthermore, the interest of increasing the number of energies, especially around 3 MeV, has been demonstrated during several ion beam energy calibration campaigns at AIFIRA facility allowing the establishment of a correction law to be applied to the terminal voltage reading of the accelerator.

These new calibration energies are reported in Table 3.

### Declaration of Competing Interest

The authors declare that they have no known competing financial interests or personal relationships that could have appeared to influence the work reported in this paper.

### Acknowledgments

The authors would like to cordially thank D. Mous and N. Podaru (HVEE) for their explanations and advices about the observed variation of the calibration curve for AIFIRA. The authors would like to thank P. Alfaut and L. Daudin (GENBG), as well as R. Babut, A. Martin and M. Pepino (IRSN) for their help during the calibration measurement respectively at AIFIRA and AMANDE facilities.

The AIFIRA facility is financially supported by CNRS, Université de Bordeaux and the Région Nouvelle Aquitaine.

### References

- [1] Y. Wang, M. Nastasi, *Handbook of Modern Ion Beam Materials Analysis*, 2nd Edn, Materials Research Society, 2009.
- [2] C. Jeynes, R. P. Webb, and A. Lohstroh *Reviews of accelerator Science And Technology* 4, 41, 2011.

- [3] G. Provasas, S. Fazinić, N. Soić, N. Vukman, D. Cosic, M. Krmpotić, M. Vuksić, A. Crnjac, R. Popočovski, L. Palada, P. Čolović, D. Dell'Aquila, I. Gašparić, D. Jelavić Malenica, T. Mijatović, M. Uroić, Nucl. Instrum. Methods Phys. Res. B 472 (2020) 36.
- [4] I. Zahradnik, M. Pomorski, L. De Marzi, D. Tromson, P. Barberet, N. Skukan, P. Bergonzo, G. Devès, J. Hérault, W. Kada, T. Pourcher, S. Saada, Phys. Status Solidi 1800383 (2018) 1.
- [5] R.C. Block, Y. Danon, F. Günsing, R.C. Haight, in: Handbook of Nuclear Engineering, Springer US, Boston, MA, 2010, pp. 1–81, [https://doi.org/10.1007/978-0-387-98149-9\\_1](https://doi.org/10.1007/978-0-387-98149-9_1).
- [6] L. Rohrer and H. Schnitter, Electrostatic Accelerators, Fundamentals and Applications pp 152-165, R.Hellborg (Ed.), Springer, 2005.
- [7] I. Rajta, I. Vajda, Gy. Gyürky, L. Csedreki, Á.Z. Kiss, S. Biri, H.A.P. van Oosterhout, N.C. Podaru, D.J.W. Mous, Nuclear Instruments and Methods in Physics Research Section A: Accelerators, Spectrometers, Detectors and Associated Equipment, 880, 125, 2018.
- [8] J.B. Marion, Rev. Mod. Phys. 38 (1966) 660.
- [9] J.C. Overley, P.D. Parker, D.A. Bromley, Nucl. Instrum. Methods 68 (1969) 61.
- [10] P. Kump, V. Ramsak, P. Rupnik, M. Vakselj, Nucl. Instrum. Methods 112 (1973) 489.
- [11] H.H. Andersen, P. Hornshøj, L. Hojsholt-Poulsen, H. Knudsen, B.R. Nielsen, R. Stensgaard, Nuclear Instruments & Methods 136 (119) (1976).
- [12] S.A. Brindhaban, P.H. Barker, M.J. Keeling, W.B. Wood, Nucl. Instrum. Methods Phys. Res. A 340 (1994) 436.
- [13] G. Meng Wang, F.G. Audi, W.J. Kondev, S. Naimi Huang, Xu. Xing, Chin. Phys. C 41 (2017), 030003.
- [14] J. B. Marion and J. L. Fowler, Fast Neutron Physics, Interscience Publishers, London, p 1867, 1960.
- [15] J.H. Kelley, R.S. Canon, S.J. Gaff, R.M. Prior, B.J. Rice, E.C. Schreiber, M. Spraker, D.R. Tilley, E.A. Wulf, H.R. Weller, Phys. Rev. C 62 (2000), 025803.
- [16] F. Ajzenberg-Selove, Nucl. Phys. A 475 (1987) 1.
- [17] J.W. Maas, E. Somorjai, H.D. Graber, C.A. Van den Wijngaart, C. Van der Leun, P. M. Endt, Nucl. Phys. A 301 (1978) 213.
- [18] P.M. Endt, C. Van der Leun, Nucl. Phys. A 214 (1973) 1.
- [19] R.O. Bondelid, E.E. Dowling-Whiting, Phys. Rev. 134 (1964) B591.
- [20] P.H. Barker, P.D. Harty, M.J. Keeling, W.B. Wood, P.A. Amundsen, Metrologia 39 (4) (2002) 4.
- [21] F. Ajzenberg-Selove, Nucl. Phys. A 523 (1991) 1.
- [22] J. Garcia Lopez, F. J. Ager, M. Barbadillo Rank, F. J. Madrigal, M. A. Ontalba, M. A. Respaldiza, and M. D. Ynsa Nuclear Instruments and Methods in Physics Research B 161-163, 1137, 2000.
- [27] P.A. Miranda, M.A. Chesta, S.A. Cancino, J.R. Morales, M.I. Dinator, J.A. Wachter, C. Tenreiro, Nucl. Instrum. Methods Phys. Res. B 248 (2006) 150.
- [28] D. Bachiller-Perea, A. Muñoz-Martin, P. Corvisiero, D. Jimenez-Rey, V. Joco, A. Maira, A. Nakbi, A. Rodriguez, J. Narros, A. Zucchiatti, Energy Procedia 41 (2013) 57.
- [29] R.H. Spear, D.C. Kean, M.T. Esat, A.M.R. Joye, M.P. Fewell, Nucl. Instrum. Methods 147 (1977) 455.
- [30] D.M. Scott, B.M. Paine, Nucl. Instrum. Methods 218 (1983) 154.
- [31] E. Andrade, C. Solis, M.F. Rocha, Nucl. Instrum. Methods Phys. Res. B 261 (2007) 553.
- [32] J.L. Colaun, G. Terwagne, C. Jeynes, Nucl. Instrum. Methods Phys. Res. B 349 (2015) 173.
- [33] V. Paneta, M. Kokkoris, A. Lagoyannis, K. Preketes-Sigalas, Nucl. Instrum. Methods Phys. Res. B 406 (2017) 108.
- [34] L. Csedreki, G. F. Ciani, Gy. Gyürky, I. Vajda, I. Rajta, Á. Z. Kiss, Nuclear Instruments and Methods in Physics Research B 478, 194, 2020.
- [35] J. Brenneisen, D. Grathwohl, M. Lickert, R. Ott, H. Röpkke, J. Schmälzlin, P. Siedle, B.H. Wildenthal, Z. Phys. A 352 (1995) 149.
- [36] V. Lamirand, V. Gressier, A. Martin, D.J. Thomas, Radiat. Meas. 45 (2010) 1112–1115.
- [37] M. Chiari, B. Melon, L. Salvestrini, M. Fonseca, E. Alves, A.P. Jesus, Nucl. Instrum. Methods Phys. Res. B 332 (2014) 355.
- [38] A. Jokar, O. Kakuee, M. Lamehi-Rachti, N. Sharifzadeh, V. Fathollahi, Nucl. Instrum. Methods Phys. Res. B 362 (2015) 138–141.
- [39] S. Sorieul, Ph. Alfaut, L. Daudin, L. Serani, Ph. Moretto, Nucl. Instrum. Methods Phys. Res. B 332 (2014) 68.
- [40] V. Gressier, J.F. Guerre-Chaley, V. Lacoste, L. Lebreton, G. Pelcot, J.L. Pochat, T. Bolognese-Milstajn, D. Champion, Radiat. Prot. Dosim. 110 (2004) 49.
- [41] V. Gressier, V. Lacoste, A. Martin, M. Pepino, Metrologia 51 (2014) 431.
- [42] V. Lacoste, Radiat. Meas. 45 (2010) 1250.
- [43] A. Cheminet, V. Lacoste, V. Gressier, G. Hubert, A. Martin, M. Pepino, J. Instrum. 7 (2012) C04007.
- [44] N. Chauvin, F. Dayras, D. Le Du, R. Meunier, Nucl. Instrum. Methods Phys. Res. A 521 (2004) 149–155.
- [45] M.A. Cognet, V. Gressier, Metrologia 47 (2010) 377.
- [46] V. Lamirand, Determination of cross sections for the production of low-energy monoenergetic neutron fields, Thesis report, University of Grenoble, 2011, <https://tel.archives-ouvertes.fr/tel-00683170>.
- [47] M. Cosack, H. Lesiecki, and J. B. Hunt, Proc. of 5th symposium on neutron dosimetry, EUR-9762 (CEC Luxembourg), I, 597, 1985.
- [48] J.F. Wilkerson, T.B. Clegg, E.J. Ludwig, Nucl. Instrum. Methods 207 (1983) 331.